Near-Real Time Tsunami Inundation Forecast for Central America : Case study of the 1992 Nicaragua Tsunami Earthquake

Yuichiro Tanioka[1)], Ulbert Gleb Grillo[2)], and Greyving Jose Arguello[2)]

1) Institute of Seismology and Volcanology, Faculty of Science, Hokkaido University, N10W8, Kita-ku, Sapporo, Japan, 062-0810

2) Nicaraguan Institute of Territorial Studies, Managua, Nicaragua.

Abstract

The large tsunami earthquake that occurred off the Pacific coast of Nicaragua in 1992 generated a large tsunami, causing significant damage along the coast. Since then, the importance of developing a real-time tsunami forecast method, particularly for tsunami earthquakes, has been recognized. In this study, a near-field tsunami inundation forecast method (NearTIF) for the Pacific coast of Central America is developed and tested on the basis of the 1992 Nicaragua tsunami earthquake case. The appropriate source model of the 1992 Nicaragua earthquake, estimated using the W-phase inversion with a depth dependent rigidity curve from a previous study, is used as a reference model to test the proposed NearTIF method. The tsunami inundation along the Pacific coast of Nicaragua is computed from the reference model of the 1992 Nicaragua earthquake. The tsunami inundation obtained using the NearTIF method matches the tsunami inundations computed from the reference model. The tsunami heights and the tsunami inundation of the 1992 Nicaragua tsunami surveyed by a previous study are roughly matched by the tsunami inundations obtained using the NearTIF method in this study. Although the computational time for the tsunami inundation from the reference source model is about 95 min, the computational time plus the database search time for the NearTIF method is approximately 2-4 min. The method presented in this study can be used as a near-real time tsunami inundation forecast method for the Pacific coast of Central America.

Key words: Tsunami inundation forecast, The 1992 Nicaragua Tsunami, Central America

1. Introduction

In 1992, a large earthquake occurred off the Pacific coast of Nicaragua and generated a large tsunami causing significant damage along the Nicaragua coast (Abe et al., 1993). The tsunami was much larger than that expected from its surface wave magnitude of M_s 7.2. Therefore, the earthquake is classified as a 'tsunami earthquake' (Satake et al., 1993). After the 1992 Nicaragua tsunami earthquake, a seismic network and the National Tsunami Warning System (NTWS) was developed in Nicaragua (Strauch et al., 2018). However, real-time tsunami forecasts using the surface wave magnitude still have a possibility to underestimate tsunami heights for tsunami earthquakes such as the 1992 Nicaragua earthquake. In 2016, the Central American Tsunami Advisory Center (CATAC) was established at the Nicaraguan Institute of Territorial Studies in Nicaragua with Japanese cooperation. This center should be completed in 2019 (Strauch et al., 2018). It is important to develop a real-time tsunami forecast method that could forecast tsunamis from tsunami earthquakes such as the 1992 Nicaragua earthquake.

Gusman and Tanioka (2014) developed a method to estimate an appropriate source model for a real-time tsunami forecast using the result from the W-phase inversion which was originally developed by Kanamori and Rivera (2008). They applied their method to the 2011 Tohoku-oki earthquake and found that the observed tsunami inundation areas and run-up heights were well explained by those numerically computed from the source model, estimated by the W-phase inversion using the first 10 min of seismic waveforms. Recently, Tanioka et al. (2017) improved their method by using the depth dependent rigidity curve and applied it for four large earthquakes that occurred off the Pacific coast of Central America, including the 1992 Nicaragua Tsunami earthquake. They showed

that the tsunami run-up heights and inundation areas for those earthquakes were well explained by those computed from the estimated source models.

Although the appropriate source models for tsunami computation are estimated, a numerical computation of tsunami inundation still requires a longer computational time than typical tsunami propagation times, unless the computation is undertaken on supercomputers, as described by Oishi et al. (2015) or Musa et al., (2018). Gusman et al. (2014) developed a reliable near-field tsunami inundation forecast method using a pre-computed tsunami inundation and pre-computed tsunami waveform database. They tested their method for the 2011 Tohoku-oki tsunami and found that the forecast results were all reliable for tsunami early warning purposes. The method was also tested at Pelabuhan Ratu in Indonesia (Setiyono et al., 2017).

In this paper, the near-field tsunami inundation forecast method developed by Gusman et al. (2014) and Tanioka et al. (2014) is improved for application to the Central America tsunami forecast system and tested for the 1992 Nicaragua tsunami earthquake. The appropriate source model of the 1992 Nicaragua earthquake estimated using the W-phase inversion with a depth dependent rigidity curve by Tanioka et al. (2017), is used to test the tsunami inundation forecast method.

2. Method

A near-field tsunami inundation forecast method (NearTIF) (Gusman et al., 2014) assumes that if different earthquakes produce the same tsunami waveforms at nearshore locations, regardless of their source mechanism, location, or arrival time, the inundation

in coastal areas from those tsunamis will have the same characteristics. The NearTIF algorithm consists of three components: (1) a pre-computed database for tsunami waveforms and tsunami inundation; (2) a near-real time tsunami numerical computation that solves the linear shallow water equations; (3) a tsunami database search engine. We describe each component in the following subsections.

2.1. Pre-computed database

The first component of the NearTIF, a pre-computed database for tsunami waveforms and tsunami inundation, is described in this section.

2.1.1. Fault models for a pre-computed database

Simple rectangular fault models of large underthrust earthquakes along the plate interface of the subducted Cocos plate off Nicaragua are used to build the tsunami waveforms and the inundation database. We distribute 10 reference points, the southern edges of those fault models, along the plate interface as shown in Figure 1. For each reference point, seven fault models with a magnitude (Mw) range from 7.0 to 8.2 are located as shown in Figure 1. In total, 70 fault models are used to construct a pre-computed database. The fault length, L (km), and fault width, W (km), are calculated from the magnitude (Mw) of the fault models using scaling relationships determined by Blaser et al. (2010), $\log L = -2.28 + 0.55Mw$ and $\log W = -1.8 + 0.45Mw$. The strikes of the fault models are set to be parallel to the trench axis (Table 1). The dip angles of the fault models are set to be 10 degrees for the shallower fault models and 15 degrees for the deeper fault models along the plate interface. The rake angle is fixed to be 90 degrees,

the pure thrust type mechanism.

The slip amounts, *D* (m) of the fault models are calculated from the following equation:

$$D = \frac{M_0}{\mu LW} \ , \ M_0 = 10^{1.5M_w+9.1} \quad (1)$$

where M_0 (Nm) is the seismic moment, *L* is the fault length in m, *W* is the fault width in m, and μ is a rigidity in N/m^2. The rigidities, μ, of the shallower and deeper faults are set to be 0.7 x 10^{10} N/m^2 and 1.0 x 10^{10} N/m^2, respectively, and are obtained from a depth dependent rigidity curve, Figure 2, suggested by Tanioka et al. (2017). They concluded that to estimate the appropriate source model for tsunami early warning using the seismic analysis, called W-phase inversion, it is important to use the depth dependent rigidity curve for the slip estimation, particularly for tsunami earthquakes. Therefore, we also used that rigidity curve for the slip estimation of fault models to construct a pre-computed database of tsunami waveforms and inundation maps. This is an improvement over the NearTIF method developed by Gusman et al. (2014).

2.1.2. Numerical simulations for a pre-computed database of tsunami inundations

Tsunamis are numerically computed from the above 70 fault models. The vertical deformation due to each fault model is computed using the equations of Okada (1985). This vertical deformation is used as the tsunami initial surface deformation. The tsunami propagation is numerically computed by solving the non-linear shallow water equations using the finite different scheme (Goto et. al., 1997). The tsunami inundation is numerically computed using the moving boundary condition (Imamura, 1996). A Manning's roughness coefficient in the non-linear shallow water equations is assumed to

be 0.025 $m^{-1/3}$. Four nested grid systems (Figure 3) are used for this tsunami simulation. For Region 1 (R1), the General Bathymetry Chart of the Oceans (GEBCO) at 30 arcsecond grid spacing is resampled to generate a 1 arc-minute (~1860 m) grid bathymetry. For Regions 2 and 3 (R2 and R3), it was interpolated to make 1/3 arc-minutes (~620 m) and 1/9 arc-minutes (~205 m) grid bathymetries, respectively. For Region 4 (R4a-e), the interpolated GEBCO 30 arcseconds bathymetry data are combined with the 3 arcseconds topography data of the Shuttle Radar Topography Mission (SRTM) to make a 1/27 arc-minutes (~69 m) grid system to compute the tsunami inundation. The tsunami inundation is computed only in five R4 regions, shown in Figure 3, to construct a tsunami inundation database. A time step of 0.5 s is used to satisfy a stability condition of all grid systems. In a case study of the 1992 Nicaragua tsunami earthquake, the tsunami survey data of the 1992 Nicaragua event (Abe et al., 1993) in five R4 regions are compared to select the best tsunami inundation.

2.1.3. Numerical simulations for a pre-computed database of tsunami waveforms

The main assumption of the NearTIF method (Gusman et al., 2014) is that tsunami waveforms at multiple virtual observation points off a tsunami inundation region represent the characteristics of tsunami wave-fields of a nearshore area including the tsunami inundation region, such as Region 4 in this study. Gusman et al. (2014) indicated that 5 to 7 virtual points are needed to capture the characteristic of the tsunami wave-field along a long coast line of about 70 km of Sendai bay. This means that if different fault models generated the same tsunami waveforms at those virtual observation points, the tsunami inundation caused by those fault models should be identical. In this study, to

capture the characteristics of the tsunami wave-field along the nearshore area, 3 - 6 virtual observation points, VOPs, in five R4 regions (Figure 4) are selected along the ocean at a depth of about 30 m because the lengths of the coast lines in five regions are between 50 km and 15 km. The tsunami waveforms at those virtual observation points are computed numerically by solving the linear shallow water equations using the finite different scheme (Goto et. al., 1997). The tsunami initial conditions for the 70 fault models and the nested grid systems are the same as for those in the previous section describing the numerical simulation for tsunami inundation. Then, the computed tsunami waveforms at those virtual observation points from 70 fault models are stored with the computed tsunami inundations in the database.

2.2. Near-real time tsunami computation

The second component of the NearTIF, a near-real time computation, is described in this section. As soon as the source model was determined using the W-phase inversion (Tanioka et al., 2017), tsunami waveforms at the virtual observation points in Figure 4 were numerically computed from the source model by solving the linear shallow water equations in near-real time. The source model determination takes about 10 - 15 min. After that, it only takes about 1 - 2 min to compute tsunami waveforms at the virtual observation points.

2.3. Tsunami inundation search engine

The third component of the NearTIF, a search engine of the database, is described in this section. For each R4 region, the first wave cycle, or the first 2000 s, of the computed

tsunami waveforms at the virtual observation points are compared with those waveforms in the database to find a fault model that generated the most similar tsunami waveforms at those points. At first, fault models that produced the maximum amplitude of within ±30% of the computed ones for all virtual observation points are selected. Then, a root mean square error (RMSE) analysis is applied to those selected fault models to find a fault model that generated the most similar waveforms. For this analysis, one optimal time shift (τ) is applied for the tsunami waveforms at all virtual observation points to obtain the minimum RMSE of the waveforms. By this time shifting, the location of the fault model does not matter for the selection of the fault model as long as the tsunami waveforms at virtual observation points are similar to each other. Finally, the pre-computed tsunami inundation of the best site-specific fault model is selected as the tsunami inundation forecast. The selected fault model is site specific, i.e., the selected fault model is only valid for a specific site with a set of virtual observation points. For each five R4 region, the searching process needs to be carried out independently.

3. Case study of the 1992 Nicaragua tsunami earthquake

The 1992 Nicaragua tsunami earthquake generated a large tsunami causing significant damage along the coast of Nicaragua. The detailed tsunami heights along the coast were surveyed by Abe et al. (1993). The tsunami was much higher than that expected from the surface wave magnitude of 7.2 or even from the moment magnitude of 7.6 - 7.7. Recently, Tanioka et al. (2017) showed that the appropriate source model for the 1992 Nicaragua event was determined using W-phase inversion with a depth dependent rigidity curve.

206 The tsunami height distribution and inundation surveyed by Abe et al. (1993) were
207 explained well by those computed from the source model.
208 In this paper, the source parameters, strike = 315.8°, dip = 9.6°, rake = 106.9°, fault
209 length = 79.4 km, fault width = 41.7 km, slip amount = 15.2 m, and central depth of 15.5
210 km, estimated by Tanioka et al. (2017) were used as the reference source model for the
211 1992 Nicaragua earthquake. Using the NearTIF method described above section, the
212 tsunami inundation at five R4 regions in Figure 4 are selected from a pre-computed
213 tsunami inundation database. The tsunami inundation was also numerically computed
214 from the reference source model solving the non-linear shallow water equations with a
215 moving boundary condition in five R4 regions. The tsunami inundation obtained using
216 our NearTIF method are compared with those directly computed from the reference
217 model to verify that our NearTIF method works well.
218
219 ***3.1. Results for the Gulf of Fonseca***
220 Figure 5 shows that the tsunami waveforms at four virtual observation points (VOP1-4
221 in Figure 4a) computed from the reference model are well explained by those selected as
222 the best scenario from the pre-computed database with a time shift of -105 s. Figure 6
223 also shows that the tsunami inundation computed from the reference models is well
224 explained by that selected as the best scenario from the database. There are small
225 differences of maximum tsunami height distribution along the coast (such as red ellipses
226 in Figure 6) which indicate limitation of our forecast method. The maximum tsunami
227 heights at Jiquilio in Figure 6, which were computed from the reference model and
228 selected as the best scenario from the database are 4.80 m and 4.33 m, respectively. These

229 are similar to each other. The maximum tsunami height surveyed at Jiquilio by Abe et al.
230 (1993) is 2.5 m, smaller than the computed and selected scenarios. This overestimation
231 compared to the surveyed maximum height could be caused either by the accuracy of the
232 reference source model or that of the topography along the coast, but not by the tsunami
233 forecast method presented in this study. The reasons for the discrepancy are discussed
234 more in discussion section.
235
236 ***3.2. Results for Corinto***
237 Figure 7 shows that the tsunami waveforms at four virtual observation points (VOP1-5
238 in Figure 4b) computed from the reference model are well explained by those selected as
239 the best scenario from the pre-computed database with a time shift of -80 s. Figure 8 also
240 shows that the tsunami inundation and tsunami height distribution computed from the
241 reference models are well explained by those selected as the best scenario from the
242 database. The maximum tsunami heights at Corinto in Figure 8, which were computed
243 from the reference model and selected as the best scenario from the database are 4.11 m
244 and 3.91 m, respectively. These are also similar to each other. The maximum tsunami
245 height surveyed at Corinto by Abe et al. (1993) is 3.9 m, consistent with the computed
246 and selected scenarios.
247
248 ***3.3. Results for El Transito***
249 The most affected area by the 1992 Nicaragua tsunami is in El Transito (Figure 4c).
250 Figure 9 shows that the tsunami waveforms at four virtual observation points (VOP1-3 in
251 Figure 4c) computed from the reference model are similar to those selected as the best

252 scenario from the pre-computed database with a time shift of -25 s. However, the
253 maximum amplitudes of waveforms from the reference model are all slightly
254 underestimated by those selected as the best scenario. Figure 10 shows that the tsunami
255 inundation area computed from the reference models is slightly underestimated by that
256 selected as the best scenario from the database. The maximum tsunami height distribution
257 from the reference model (Figure 10 right) is also slightly underestimated by that from
258 the best scenario (Figure 10 center). The maximum tsunami height at El Transito
259 computed from the reference model, 14.1 m, is slightly underestimated by that selected
260 as the best scenario, 12.8 m. Those results are expected because the maximum amplitudes
261 of tsunami waveforms were slightly underestimated at virtual observation points (Figure
262 9). The maximum tsunami height surveyed at El Transito by Abe et al. (1993) is 9.9 m,
263 slightly smaller than both the computed and selected scenarios. The tsunami inundation
264 surveyed by Abe et al. (1993) is also shown Figure 10 and explained by those computed
265 from the reference model and also selected as the best scenario from the database.
266
267 ***3.4. Results for Masachapa***
268 Figure 11 shows that the tsunami waveforms at four virtual observation points (VOP1-
269 5 in Figure 4d) computed from the reference model are explained by those selected as the
270 best scenario from the pre-computed database with a time shift of -5 s. However, the
271 maximum amplitudes of waveforms from the reference model are all slightly
272 underestimated by those selected as the best scenario for Masachapa, too. Figure 12 also
273 shows that the tsunami inundation computed from the reference models is explained by
274 that selected as the best scenario from the database. The maximum tsunami height

distribution from the reference model (Figure 12 right) is slightly underestimated by that from the best scenario (Figure 12 center). Therefore, the maximum tsunami heights at Masachapa computed from the reference model, 8.36 m, is also underestimated by that selected as the best scenario, 6.58 m. The maximum tsunami height surveyed at Masachapa by Abe et al. (1993) is 6.2 m, which is slightly smaller than that from the reference model and is consistent with that from the best scenario.

3.5. Results for El Astilleo

Figure 13 shows that the tsunami waveforms at four virtual observation points (VOP1-6 in Figure 4e) computed from the reference model are well explained by those selected as the best scenario from the pre-computed database with a time shift of 75 s. Figure 14 also shows that the tsunami inundation computed from the reference models is explained by that selected as the best scenario from the database. However, there are small differences of maximum tsunami height distributions along the coast (such as red ellipses in Figure 13) which indicate limitation of our forecast method. The maximum tsunami heights at La Salinas in Figure 11 which were computed from the reference model and selected as the best scenario from the database are 4.66 m and 4.22 m, respectively. These are slightly smaller than the maximum tsunami height of 6.7 m surveyed at by Abe et al. (1993). The maximum tsunami heights at Popoyo computed from the reference model and selected as the best scenario from the database are 4.05 m and 3.77 m, respectively, again slightly smaller than the maximum tsunami height of 5.6 m surveyed at by Abe et al. (1993). The reasons for those discrepancies are discussed in the following discussion section.

298

299 **4. Discussions**

300

301 In this paper, the simple rectangular fault model estimated by Tanioka et al, (2017) was
302 used as the reference model for the 1992 Nicaragua tsunami case study because the
303 surveyed tsunami inundation data (Abe at al., 1993) were roughly explained by the
304 tsunami inundation computed from the model. Tsunamis computed from complicated
305 source models can be explained more detail of tsunami inundation pattern. However, in
306 Central America, it is still difficult to estimate an appropriate slip distribution of a large
307 earthquake before a large tsunami hits the coast. Therefore, the rectangular fault model
308 (Tanioka et al., 2017) should be the best choice for this study.

309 The maximum tsunami heights selected as the best scenario from the database were
310 similar to those computed from the reference model. The differences are within 22% of
311 those computed from the reference model (Table 2). However, the observed tsunami
312 heights by Abe et al. (1992) were slightly different from those computed from the
313 reference model, especially at Jiquilio in Gulf of Fonseca region and La Salinas. The
314 observed maximum tsunami height at Jiquilio, 2.5 m, was overestimated by the computed
315 heights from the reference model, 4.80 m, and the selected heights as the best scenario,
316 4.33 m. The observed maximum tsunami height at La Salinas, 6.7 m, was underestimated
317 by that from the reference model, 4.66 m, and that from the best scenario, 4.22 m. First
318 reason for these discrepancies is that the actual source model of the 1992 Nicaragua
319 earthquake was not completely represented by a single rectangular fault model. It will be
320 improved in future when more appropriate source models of large earthquakes are quickly

321 determined for tsunami early forecast purpose in Central America. Second reason may be
322 that the SRTM topography data are not accurate enough to represent the topography in
323 those tsunami inundation area. It can be improved if the accurate local topography data
324 are available.
325 The limitation of the method in this study which indicated by the differences between
326 tsunami heights selected as the best scenario from the database and computed tsunami
327 heights from a reference fault model (Table 2) can be improved by using larger number
328 of the various scenarios in the database. Various tsunami waveforms at virtual
329 observation points from scenarios are needed to improve an accuracy of our forecast
330 method. However, the computational time to select the best scenario becomes also larger
331 when the number of scenarios becomes larger. It is important to make an appropriate
332 database which efficiently includes the most probable scenarios. This study clearly
333 indicates that scenarios of which slip amounts were estimated using the depth dependent
334 rigidity should be included in a database to forecast tsunami heights of tsunami
335 earthquakes such as the 1992 Nicaragua tsunami earthquake.
336
337 **5. Conclusions**
338
339 The tsunami inundations along the Pacific coast of Nicaragua computed from the
340 reference source model of the 1992 Nicaragua earthquake were explained by the tsunami
341 inundation selected by the NearTIF method using pre-computed tsunami waveforms at
342 virtual observation points near the coast of inundation and pre-computed tsunami
343 inundation constructed in the database. The tsunami heights and the tsunami inundation

of the 1992 Nicaragua tsunami surveyed by Abe et al. (1993) were roughly matched by the tsunami inundation selected by the NearTIF method in this study. Although the computational time for the tsunami inundation from the reference source model was about 95 min, the computational time plus the database search time for the NearTIF method should be about 2 - 4 min. To obtain the appropriate source model using the method suggested by Tanioka et al. (2017), it may take about 10 - 20 min depending on the station distribution of the broadband seismometers. The survey data by Abe et al. (1993) indicated that the 1992 Nicaragua tsunami arrived at the coast about 44-55 minutes after the earthquake. Computed tsunami from the reference model arrives at the virtual observation points about 43-60 minutes after the origin time. Therefore, the method is feasible for near-real time tsunami inundation forecasting along the Pacific coast in Central America.

Acknowledgments

We thank three anonymous reviewers for useful comments to improve the manuscript. We would like to thank Editage (www.editage.com) for English language editing. This study was supported by the Ministry of Education, Culture, Sports, Science and Technology (MEXT) of Japan, under its Earthquake and Volcano Hazards Observation and Research Program.

References

Abe, K., Tsuji, Y., Imamura, F., Katao, H., Iio, Y., and Estrada, F., (1993). Field survey of the Nicaragua earthquake and tsunami of September 2, 1992. Earthquake

Research Institute, University of Tokyo, 68, 23–70. (in Japanese).

Blaser, L., Kru¨ger, F., Ohrnberger, M., and Scherbaum, F., (2010). Scaling relations of earthquake source parameter estimates with special focus on subduction environment. Bulletin of the Seismological Society of America, 100(6), 2914–2926. doi:10.1785/0120100111.

Goto, C., Ogawa, Y., Shuto, N., and Imamura, F., (1997). IUGG/IOC time project: Numerical method of tsunami simulation with the leap-flog scheme, IOC of UNESCO, manuals and guides 35.

Gusman, A. R., and Tanioka, Y., (2014). W phase inversion and tsunami inundation modeling for tsunami early warning: case study for the 2011 Tohoku event. Pure and Applied Geophysics, 171(7), 1409–1422.

Gusman, A. R., Tanioka, Y., MacInnes, B. T., and Tsushima, H., (2014). A methodology for near-field tsunami inundation forecasting: application to the 2011 Tohoku tsunami. Journal of Geophysical Research, 119(11), 8186–8206.

Kanamori, H., & Rivera, L. (2008). Source inversion of W phase: speeding up seismic tsunami warning. Geophysical Journal International, 175(1), 222–238.

Musa, A., Matsuoka, H., Watanabe, O., Murashima, Y., Koshimura, S., Hino, R., Ohta, Y., and Kobayashi, H., (2015). A realtime tsunami inundation forecast system for tsunami disaster prevention and mitigation. The International Conference on High Performance Computing, Networking, Storage and Analysis (extended abstract).

Oishi, Y., Imamura, F., & Sugawara, D. (2015). Near-field tsunami inundation forecast using the parallel TUNAMI-N2 model: Application to the 2011 Tohoku-Oki earthquake combined with source inversions. Geophysical Research Letters, 42(4),

1083–1091.

Okada, Y., (1985). Surface deformation due to shear and tensile faults in a half-space. Bulletin of the Seismological Society of America, 75, 1135–1154.

Satake, K., Bourgeois, J., Abe, K., Abe, K., Tsuji, Y., Imamura, F., Lio, Y., Katao, H., Noguera, E. and Estrada, F., (1993). Tsunami field survey of the 1992 Nicaragua earthquake, EOS, pp. 145–157.

Setiyono, U., Gusman A.R., Satake K., and Fujii Y., (2017). Pre-computed tsunami inundation database and forecast simulation in Pelabuhan Ratu, Indonesia, Pure and Applied Geophysics, 174, 3219-3235, doi:10.1007/s00024-017-1633-8.

Strauch, W., Talavera E., Tenorio V., Ramirez J., Arguello G., Herrera M., Acosta A., and Morales A., (2018), Toward an Earthquake and Tsunami Monitoring and Early Warning System for Nicaragua and Central America, Seismological Research Letters, 89, 400-406, doi: 10.1785/0220170193.

Tanioka, Y., Miranda, G.J.A., Gusman A.R., and Fujii Y., (2017). Method to Determine Appropriate Source Models of Large Earthquakes Including Tsunami Earthquakes for Tsunami Early Warning in Central America Pure and Applied Geophysics, 174, 3237-3248, doi:10.1007/s00024-017-1630-y

Table 1 The fault parameters and rigidity for fault models shown in Figure 1.

fault no	location at the southern corner of fault model		shallowest depth (km)	strike (°)	dip (°)	rigidity (x 10^{11} N/m^2)
	longitude (°W)	latitude (°N)				
1	86.69	10.31	10.0	321.0	10.0	0.7
2	87.03	10.73	10.0	318.0	10.0	0.7
3	87.44	11.09	10.0	315.0	10.0	0.7
4	87.85	11.73	10.0	309.0	10.0	0.7
5	88.31	11.73	10.0	301.0	10.0	0.7
6	86.49	10.52	15.0	321.0	15.0	1.0
7	86.82	10.95	15.0	318.0	15.0	1.0
8	87.20	11.34	15.0	315.0	15.0	1.0
9	87.62	11.68	15.0	309.0	15.0	1.0
10	88.07	11.99	15.0	301.0	15.0	1.0

Table 2 Comparison of the maximum tsunami heights surveyed by Abe et al. (1993), those computed from the reference model (A), and those selected as the best scenario (B).

location	Maximum tsunami heights (m)			Percentage of difference, (A-B)/A*100
	measured	computed from the reference model (A)	selected as the best scenario (B)	
Jiquilio	2.5	4.80	4.33	9.79%
Corinto	3.9	4.11	3.91	4.87%
El Transito	9.9	14.1	12.8	9.22%
Masachapa	6.2	8.36	6.58	21.3%
La Salinas	6.7	4.66	4.22	9.44%
Popoyo	5.6	4.05	3.77	6.91%

Figure Captions

Figure 1. Map of the fault models to construct the pre-computed tsunami waveforms and inundations. Ten orange dots show the location of the southern corner of fault models. The red rectangles show the fault models from M7.0, 7.2, 7.4, 7.6, 7.8, 8.0, and 8.2 for the orange dot 1.

Figure 2. The depth dependent rigidity curve suggested by Tanioka et al. (2017). Red lines show the rigidities for 10 km and 15 km depths.

Figure 3. Four nested grid systems (R1, R2, R3, and R4) for the tsunami numerical simulation. Five areas were selected for tsunami inundation simulation, Gulf of Fonseca (R4.a), Corinto (R4.b), El Transito (R4.c), Masachapa (R4.d), and El Astilleo (R4.e)

Figure 4. Locations of virtual observation points, red triangles, where pre-computed tsunami waveforms were stored in the database for a) Gulf of Fonseca (R4.a), b) Corinto (R4.b), c) El Transito (R4.c), d) Masachapa (R4.d), and e) El Astilleo (R4.e) in Figure 3.

Figure 5. The results for Gulf of Fonseca (R4a). (left and center) Comparison of tsunami waveforms at four virtual points computed from the reference fault model of the 1992 Nicaragua earthquake (*blue*) and those selected as the best scenario from the pre-

444 computed database (*red*). (right) Optimum time shift and RMSE.

445

446 Figure 6. The results of tsunami inundations for Gulf of Fonseca (R4a). (left) Bathymetry
447 and topography. (center) Tsunami inundation selected as the best scenario from the
448 pre-computed database. (right) Tsunami inundation computed from the reference fault
449 model.

450

451 Figure 7. The results for Corinto (R4b). (left, center, and right top) Comparison of tsunami
452 waveforms at five virtual points computed from the reference fault model of the 1992
453 Nicaragua earthquake (*blue*) and those selected as the best scenario from the pre-
454 computed database (*red*). (right bottom) Optimum time shift and RMSE.

455

456 Figure 8. The results of tsunami inundations for Corinto (R4b). (left) Bathymetry and
457 topography. (center) Tsunami inundation selected as the best scenario from the pre-
458 computed database. (right) Tsunami inundation computed from the reference fault
459 model.

460

461 Figure 9. The results for El Transito (R4c). (left, and right top) Comparison of tsunami
462 waveforms at three virtual points computed from the reference fault model of the 1992
463 Nicaragua earthquake (*blue*) and those selected as the best scenario from the pre-
464 computed database (*red*). (right bottom) Optimum time shift and RMSE.

465

466 Figure 10. The results of tsunami inundations for El Transito (R4c). (left) Bathymetry and

topography. (center) Tsunami inundation selected as the best scenario from the pre-computed database. (right) Tsunami inundation computed from the reference fault model. Solid lines show the limit of the tsunami inundation surveyed by Abe et al. (1993). The detailed tsunami inundation and run-up heights due to the 1992 Nicaragua earthquake (Abe et al., 1993) are shown in the bottom.

Figure 11. The results for Masachapa (R4d). (left, center, and right top) Comparison of tsunami waveforms at five virtual points computed from the reference fault model of the 1992 Nicaragua earthquake (*blue*) and those selected as the best scenario from the pre-computed database (*red*). (right bottom) Optimum time shift and RMSE.

Figure 12. The results of tsunami inundations for Masachapa (R4d). (left) Bathymetry and topography. (center) Tsunami inundation selected as the best scenario from the pre-computed database. (right) Tsunami inundation computed from the reference fault model.

Figure 13. The results for El Astilleo (R4e). (left, center, and right top) Comparison of tsunami waveforms at five virtual points computed from the reference fault model of the 1992 Nicaragua earthquake (*blue*) and those selected as the best scenario from the pre-computed database (*red*). (right bottom) Optimum time shift and RMSE.

Figure 14. The results of tsunami inundations for El Astilleo (R4e). (left) Bathymetry and topography. (center) Tsunami inundation selected as the best scenario from the pre-

computed database. (right) Tsunami inundation computed from the reference fault model.

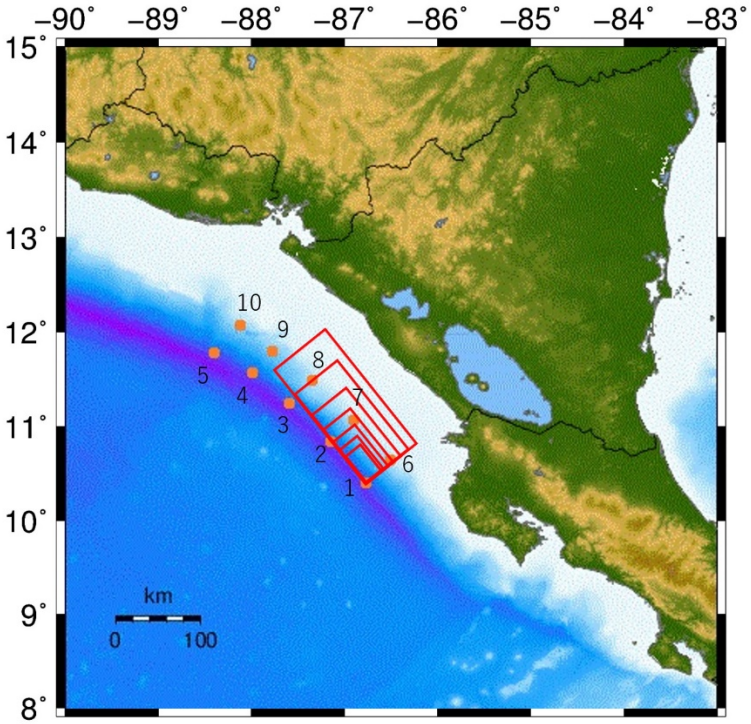

Figure 1.

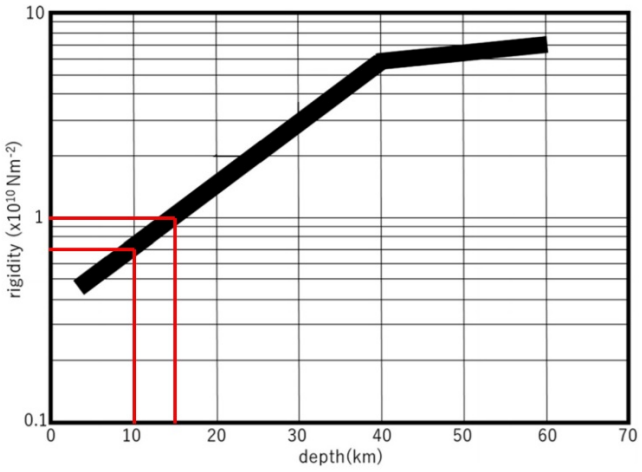

Figure 2.

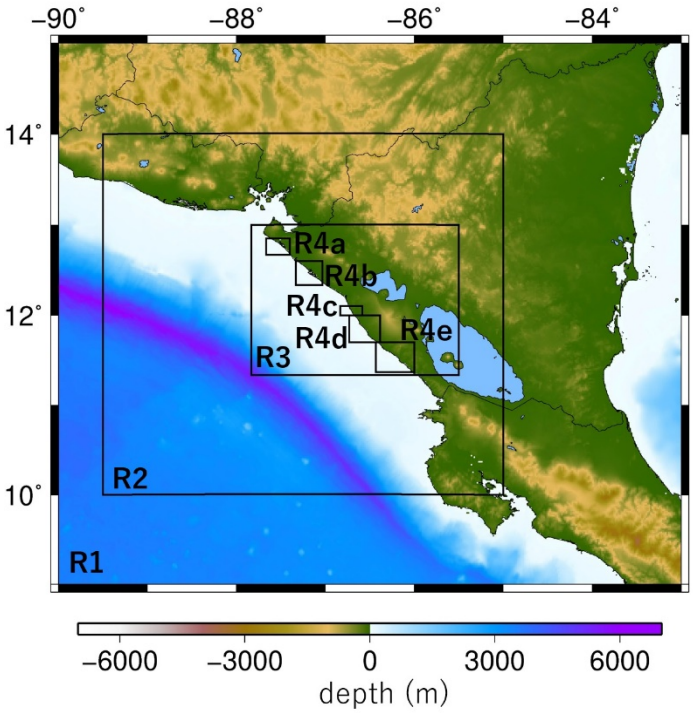

498

499 Figure 3.

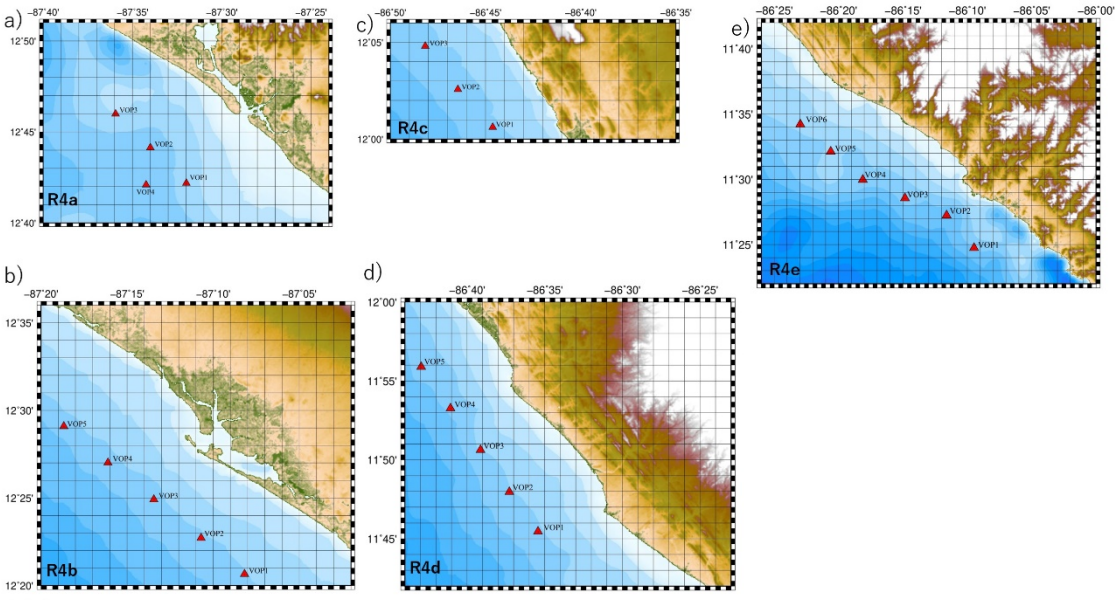

500

501 Figure 4.

502

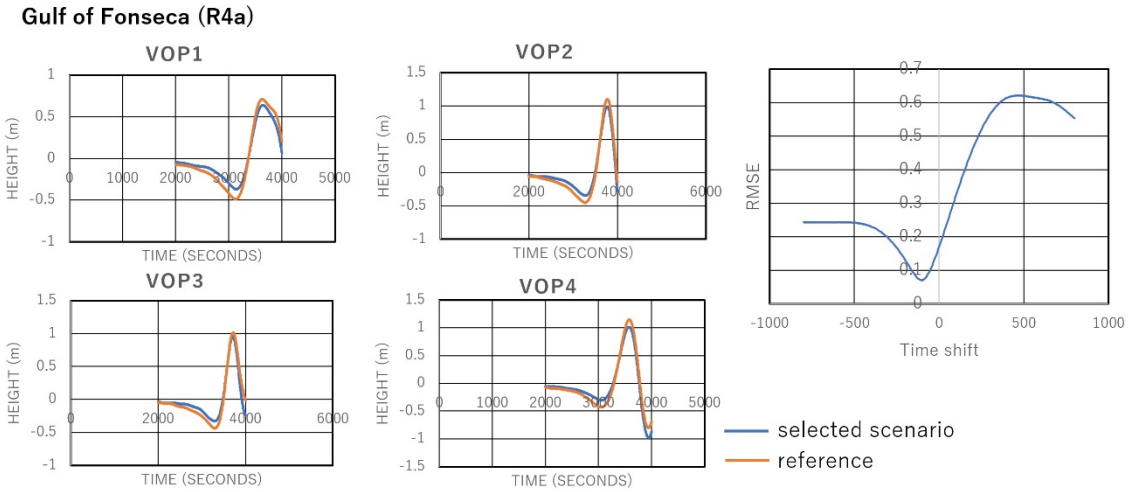

503

504 Figure 5.

505

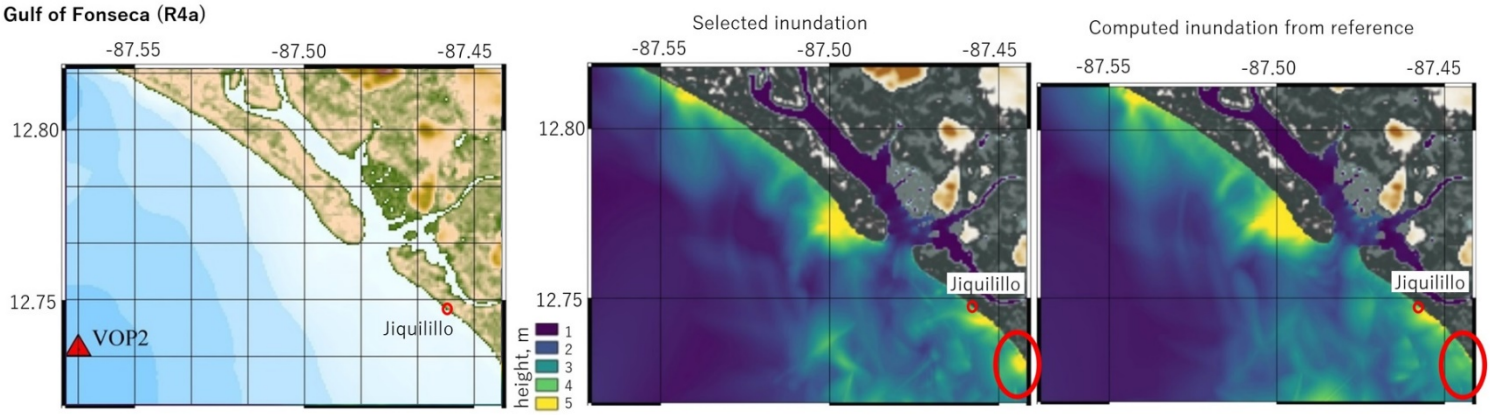

506 Figure 6.

507

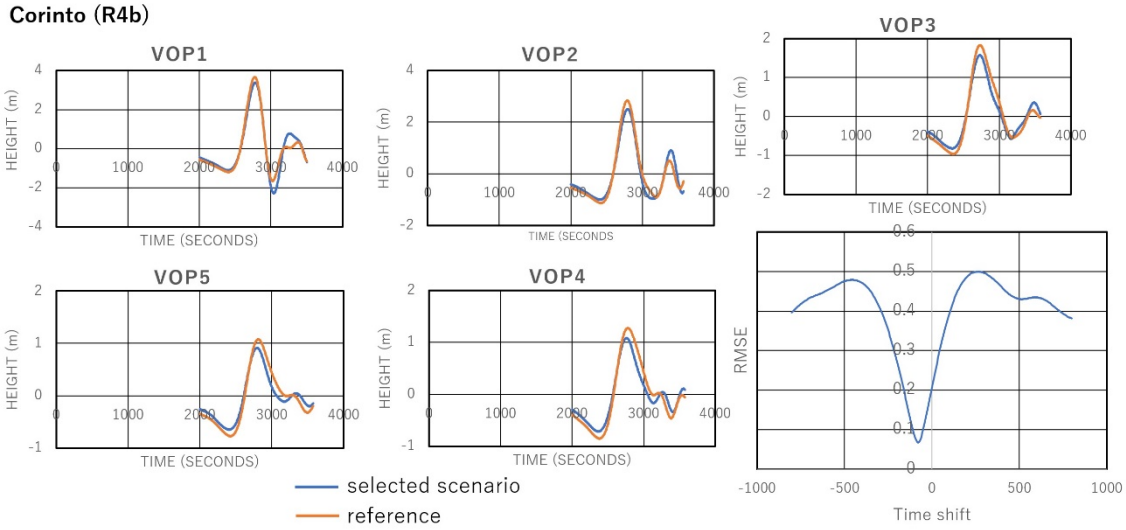

508

509 Figure 7.

510

511

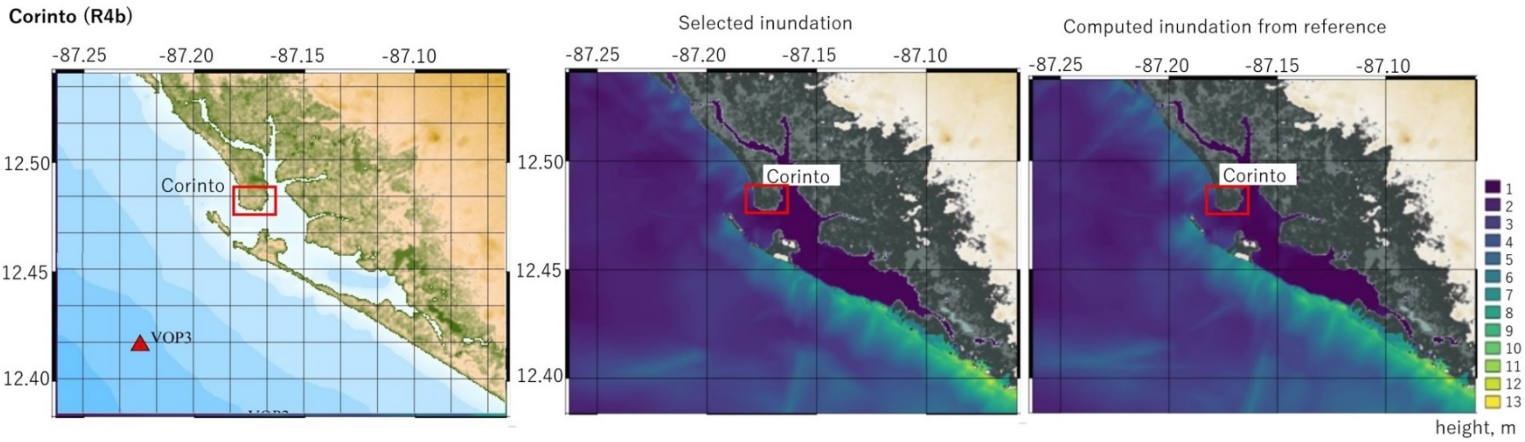

512 Figure 8.

513

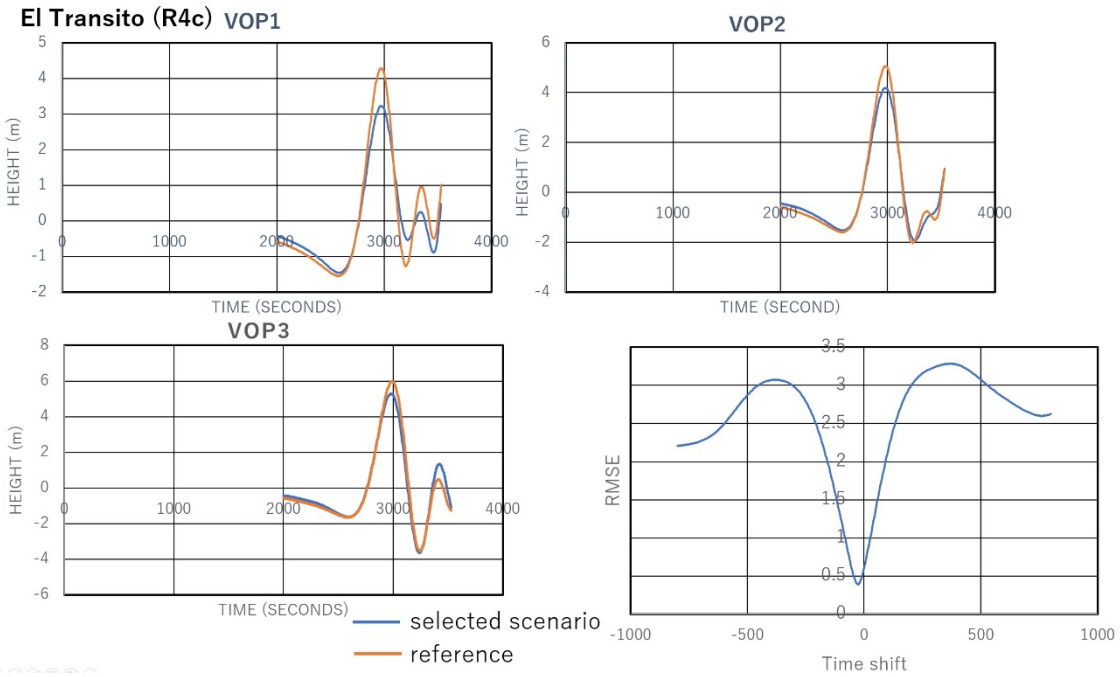

514

515 Figure 9.

516

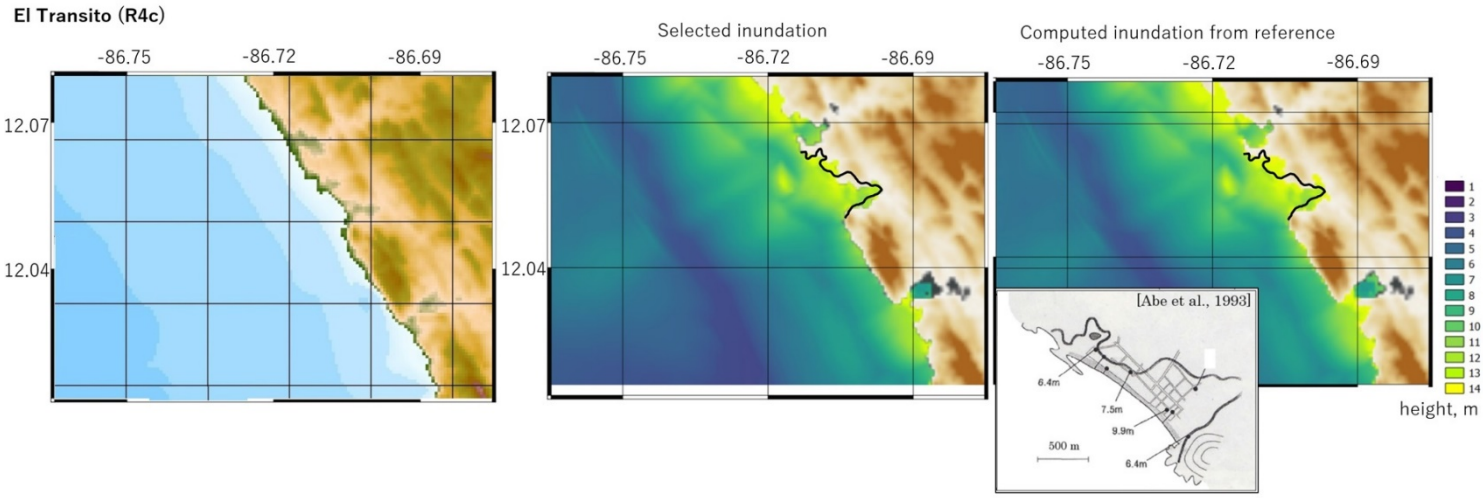

517 Figure 10.

518

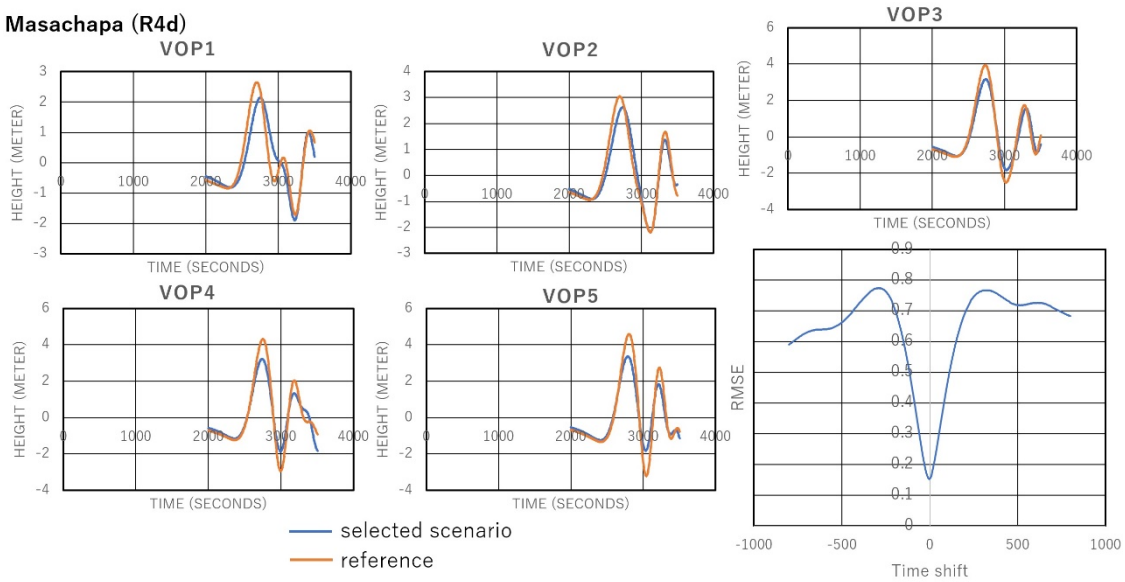

519

520 Figure 11

521

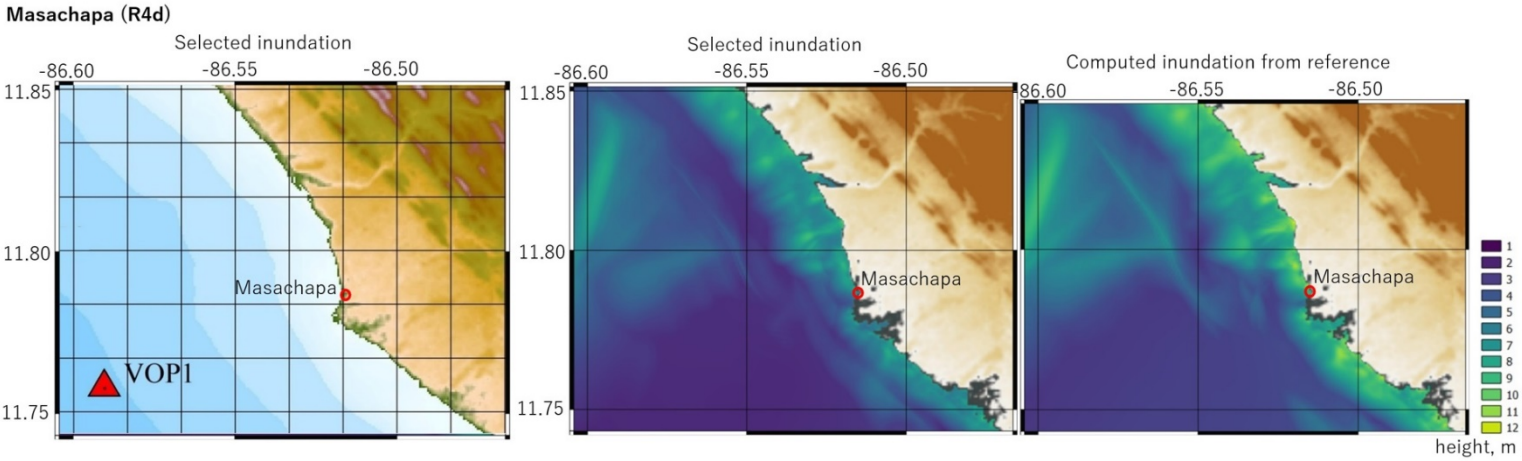

522 Figure 12.

523

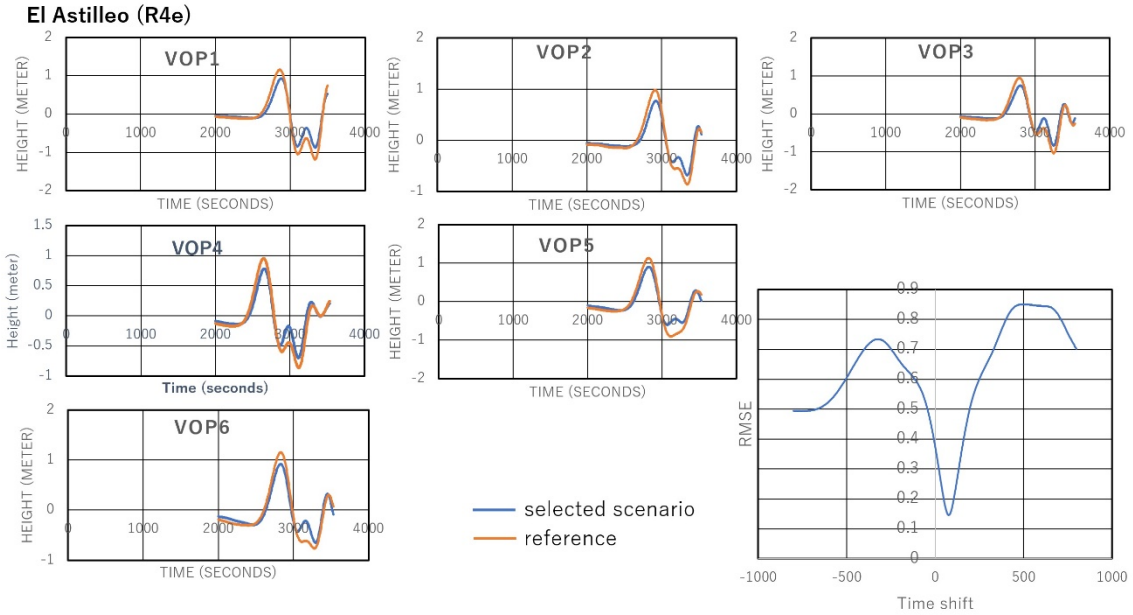

524

525

526 Figure 13.

527

528

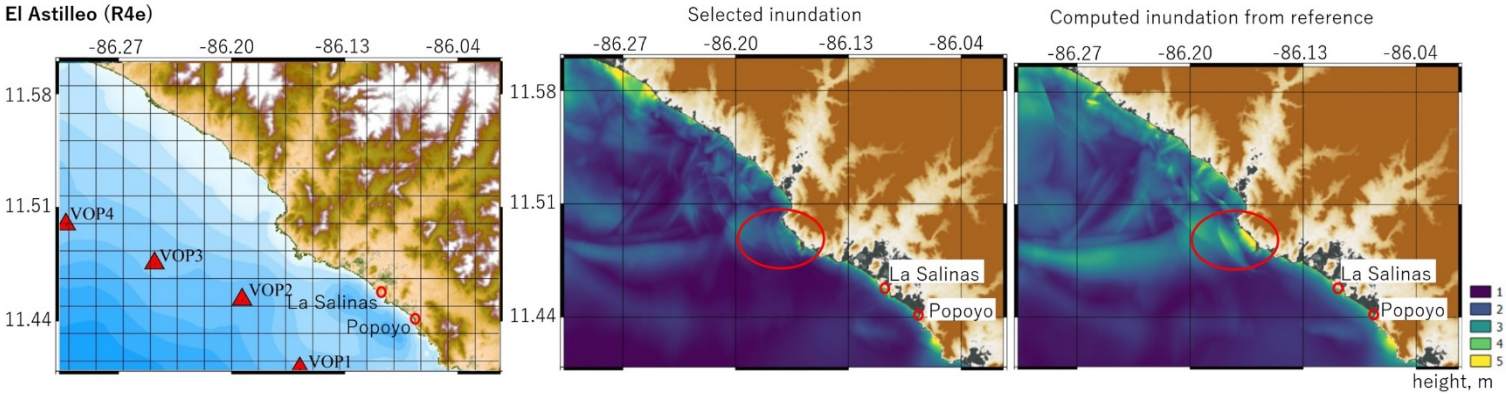

529 Figure 14.